Novel photocatalysts Pt/Cd$_{1-x}$Zn$_x$S/ZnO/Zn(OH)$_2$: Activation during hydrogen evolution from aqueous solutions of ethanol under visible light

Ekaterina A. Kozlova [a,b,c,*], Svetlana V. Cherepanova [a,b,c], Dina V. Markovskaya [a,b,c], Andrey A. Saraev [a,b], Evgeny Yu. Gerasimov [a,b,c], Valentin N. Parmon [a,b]

[a] Boreskov Institute of Catalysis SB RAS, Pr. Ak. Lavrentieva, 5, Novosibirsk 630090, Russia
[b] Novosibirsk State University, Pirogova Str. 2, Novosibirsk 630090, Russia
[c] Educational Center for Energy Efficient Catalysis in Novosibirsk State University, Pirogova Str. 2, Novosibirsk 630090, Russia

A B S T R A C T

The transformations of single-phase Pt/Cd$_{1-x}$Zn$_x$S and multiphase Pt/Cd$_{1-x}$Zn$_x$S/ZnO/Zn(OH)$_2$ and Pt/Cd$_{1-x}$Zn$_x$S/Zn(OH)$_2$ during photocatalytic hydrogen evolution from aqueous solutions of ethanol under visible light (λ = 450 nm) were investigated. Cyclic tests including long-term experiments were conducted for all photocatalysts. The photocatalysts were investigated before and after the photocatalytic reaction by X-ray diffraction (XRD), X-ray photoelectron spectroscopy (XPS), and UV–vis spectroscopy techniques. Activation during photocatalytic hydrogen evolution was observed for all multiphase photocatalysts, whereas single phase Pt/Cd$_{1-x}$Zn$_x$S was shown to exhibit a strong deactivation. The activation is likely caused by the formation of the ϵ-Zn(OH)$_2$ phase in a basic medium. The highest exhibited rate of hydrogen evolution on the composite photocatalyst was 3400 μmol g^{-1} h^{-1}, and stability during ten 5-hour photocatalytic runs was observed.

© 2015 Elsevier B.V. All rights reserved.

1. Introduction

The rapid depletion of natural raw hydrocarbons (oil, gas, and coal) has presented an acute need to identify and develop alternative energy sources [1]. The unique properties of hydrogen make it a versatile and environmentally friendly chemical energy carrier, suitable for use in all types of heat engines and power generation devices [2]. Great efforts have currently devoted to the production of hydrogen from renewable resources, including biomass catalytic steam reforming/gasification and photoelectrochemical or enzymatic approaches [3,4]. The photocatalytic splitting of water using the energy of the visible part of solar light is a very attractive approach to hydrogen production [5,6]. The application of organic substances as electron donors looks more advantageous from a practical perspective because most water pollutants are organic compounds, and the production of hydrogen in this case can be combined with the purification of water [7]. Earlier, photocatalytic

destruction of carboxylic and chlorinated carboxylic acids [8–10], organophosphorous compounds [7], some azo-dyes [11,12] with hydrogen evolution was carried out. Also, the use of biomass-derived oxygenated compounds, such as ethanol [13], methanol [14], glycerol [13,15], isopropanol [16], and sugars [13] as electron donors looks very prospective because in this case hydrogen can be produced with the use of a photocatalyst and three abundant and renewable sources: biomass, solar light, and water [13,14].

Metal sulfides have attracted considerable attention as photocatalysts for hydrogen evolution under visible light because of their appropriate band gaps and catalytic functions [17–19]. Composite systems that consist of more than two semiconductor components have been considered promising because they can compensate for the disadvantages of the individual components and induce synergistic effects, such as strong visible light absorption and improved photostability [20,21]. Recently, we showed that the composite photocatalysts Pt/Cd$_{1-x}$Zn$_x$S/ZnO/ϵ-Zn(OH)$_2$ possess significant activity in the evolution of hydrogen from aqueous solutions of ethanol, and their photocatalytic activity increases with ϵ-Zn(OH)$_2$ content [22]. However, zinc hydroxide is believed to have a low stability because the evolution of hydrogen from aqueous solutions of organic compounds on CdS-based catalysts is usually conducted in

Table 1
Properties of the photocatalysts used for the experiments on hydrogen evolution.

Photocatalyst	Synthesis			Phase composition	%, mol	ACS[d], nm	λ[e], nm	S_{BET}, m²/g	Pt, wt%	AQE[f], %
	n_{Na2S}[a]	n_{Na2S}[b]	DT[c], °C							
A	0.50	0.37	80	$Cd_{0.65}Zn_{0.35}S$	37	3.5	468	120	0.44	7.2
				ZnO	3	40				
				ϵ-$Zn(OH)_2$	45	>100				
				2D β-$Zn(OH)_2$	15	17				
B			70	$Cd_{0.65}Zn_{0.35}S$	37	3.5	470	125	0.75	4.5
				2D β-$Zn(OH)_2$	19	19				
C	0.70	0.60	90	$Cd_{0.4}Zn_{0.6}S$	60	3	435	135	1.1	4.7
				ZnO	11	50				
				2D β-$Zn(OH)_2$	6	10				
D	0.30	0.24		$Cd_{0.75}Zn_{0.25}S$	24	3.5	476	105	1.1	12.4
				ZnO	62	70				
				2D β-$Zn(OH)_2$	10	17				
$Cd_{0.6}Zn_{0.4}S$	2.5	1.0	70	$Cd_{0.6}Zn_{0.4}S$	100	<2	527	147	0	0.2
1%Pt $Cd_{0.6}Zn_{0.4}S$				$Cd_{0.6}Zn_{0.4}S$	100	<2	528		1.0	1.7

[a] Amount of Na_2S added at stage II.
[b] Amount of Na_2S that reacted at stage II (calculated using phase composition of photocatalysts).
[c] Drying temperature.
[d] Average crystalline size.
[e] Adsorption edge.
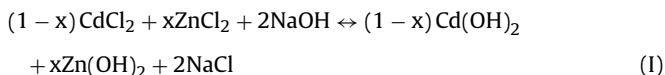[f] Calculated at the highest rate of hydrogen evolution.

alkaline media [23]. Thus, the aim of this research was to study the stability of the composite photocatalysts $Pt/Cd_{1-x}Zn_xS/ZnO/\epsilon$-$Zn(OH)_2$ in hydrogen evolution under visible light.

To date, it has been often observed that the kinetic curves of hydrogen production from aqueous solutions of organic compounds have an apparent induction period [20,24–27]. However, there is no consensus on the mechanism of this activation. In this research, we seek to investigate the transformation of single-phase $Pt/Cd_{1-x}Zn_xS$ and multiphase $Pt/Cd_{1-x}Zn_xS/ZnO/Zn(OH)_2$ photocatalysts during photocatalytic hydrogen evolution from aqueous solutions of ethanol under visible light ($\lambda = 450$ nm). Cyclic tests, including long-term experiments, have been conducted for all photocatalysts. The investigations of the composite photocatalysts before and after photocatalytic hydrogen evolution by XRD and XPS provide new knowledge about the active component of the catalyst.
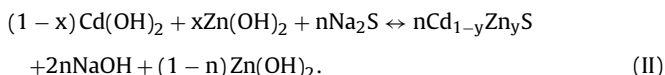
2. Experimental details

2.1. Photocatalyst synthesis

The composite photocatalysts $Cd_{1-x}Zn_xS$, $Cd_{1-x}Zn_xS/Zn(OH)_2$, and $Cd_{1-x}Zn_xS/ZnO/Zn(OH)_2$ were synthesized according to the technique described in detail elsewhere [22,27]. The synthesis technique includes the formation of the mixture of cadmium and zinc hydroxides from a mixture of soluble metal salts

$$(1 - x)CdCl_2 + xZnCl_2 + 2NaOH \leftrightarrow (1 - x)Cd(OH)_2$$
$$+ xZn(OH)_2 + 2NaCl \tag{I}$$

with further addition of sodium sulfide (II)

$$(1 - x)Cd(OH)_2 + xZn(OH)_2 + nNa_2S \leftrightarrow nCd_{1-y}Zn_yS$$
$$+ 2nNaOH + (1 - n)Zn(OH)_2. \tag{II}$$

If $n < 1$ and $n > 1 - x$, the reaction results in a mixture of $Cd_{1-y}Zn_yS$ and $Zn(OH)_2$, where y is equal to $(n + x - 1)/n$. The variation in the phase content was achieved by the use of the different amounts of sodium sulfide at stage (II). For all experiments, x was equal to 0.8; values of n are given in Table 1. Drying temperature varied from 70 to 90 °C.

Platinum was deposited by the soft chemical reduction technique. This technique was described in detail elsewhere [22,27].

The calculated amount of platinum was 1.0 wt% for all photocatalysts, whereas the real content of deposited platinum measured with the use of X-ray fluorescence spectroscopy varied from 0.44 to 1.1 wt%. The phase composition of the photocatalysts and their abbreviations are given in Table 1.

2.2. Catalyst characterization

The elemental analysis was carried out on an ARL Perform'X 3.6 kW X-ray fluorescence spectrometer equipped with an X-ray tube with a rhodium anode.

The qualitative and quantitative phase composition was analyzed by X-ray diffraction. The XRD patterns were recorded on a D8 Advance diffractometer (Bruker, Germany) using $CuK\alpha$ radiation. The scanning was performed in the 2θ range from 15° to 65° with step of 0.05° and acquisition time of 10 s at each point. The average crystallite size was calculated using the Scherrer equation. The quantitative phase composition determination was described in detail earlier [22]. Parameter y in $Cd_{1-y}Zn_yS$ was calculated using a calibration curve showing the position of the first $Cd_{1-y}Zn_yS$ peak in the dependence on the Zn content. The plot was calculated using mixed sulphides with known compositions. Calculated parameter y was in a good agreement with the formula $y = (n + x - 1)/n$ (Eq. II). Molar contents of oxides and sulfides were calculated with the use of mechanical mixtures and molar contents of oxides and hydroxides were calculated with use of simulations by the TOPAS package (General Profile and Structure Analysis Software for Powder Diffraction Data, Bruker AXS GmBH, Karlsruhe, Germany) [22].

The specific surface areas of the photocatalysts were obtained from the low-temperature N_2 adsorption–desorption (N_2 adsorption at 77 K) using an ASAP 2400 apparatus.

The diffuse reflectance spectra (Fig. A.1a of Supplementary data) were recorded on a Perkin Elmer UV/VIS spectrometer Lambda 35 with an integrating sphere RSA-PE-20 (Labsphere, USA) in a wavelength range from 200 to 1100 nm. Magnesium oxide was used as a reference. The Taucs' functions $F(R)^2(h\nu)^2$ versus $h\nu$ were plotted to estimate the adsorption edge (Fig. A.1b of Supplementary data).

XPS measurements was performed using a photoelectron spectrometer (SPECS Surface Nano Analysis GmbH, Germany) equipped with an X-ray source XR-50 M, an ellipsoidal crystal monochromator FOCUS-500, and a hemispherical electron energy analyzer

PHOIBOS-150. The valence band and core-level spectra were obtained using monochromatic Al $K\alpha$ radiation. The charge correction was performed by setting the $C1s$ peak at 284.8 eV resulting from adventitious hydrocarbons.

2.3. Catalytic activity measurements

Studies on the photocatalytic evolution of hydrogen from an aqueous solution of ethanol were carried out by the method described earlier [22]. A water suspension with a catalyst, ethanol, and NaOH was placed into a sealed reactor and illuminated with a 450-nm LED (32.7 mV/cm^2, S = 6.3 cm^2). Fig A.2 of Supplementary data represents the reaction set-up. Before the reaction, the suspension was treated in an ultrasonic bath for 10 min and bubbled with argon for 20 min to remove oxygen. The ethanol concentration was 10 vol%, the concentration of NaOH was 0.1 M, the catalyst concentration was 0.5 g L^{-1}, the suspension volume was 100 mL, temperature was 20 °C. The concentration of evolved hydrogen was measured with a gas chromatograph LKhM-8 (Russia) equipped with a thermal conductivity detector and a zeolite column; argon was used as the carrier gas; methanizer was used for carbon oxides analysis.

To calculate the apparent quantum efficiency (AQE) of the photocatalysts, the number of photons used for the hydrogen formation was divided by the whole number of photons reached the sample. The participation of at least two photons is necessary to generate one turnover of the hydrogen formation. The calculated photon flux was 46 μEinstein min^{-1}. Therefore, the AQE of the sample can be found from the formula AQE(%) = $(2 \times W/46) \times 100$%, where W is the rate of hydrogen formation in μmol/min.

3. Results and discussion

3.1. Activation of multiphase photocatalysts during hydrogen production

It has been shown in our earlier works [22,27] and previously published articles by other groups [24–26] that the kinetic curves of hydrogen production from aqueous solutions of organic compounds on platinized photocatalysts have an apparent induction period. To understand this phenomenon, we conducted several consecutive runs of hydrogen evolution under visible light on different platinized photocatalysts (Table 1) coupled with XRD and XPS investigations of the samples before and after hydrogen evolution.

The multiphase platinized photocatalysts Pt/Cd$_{1-x}$Zn$_x$S/ZnO/Zn(OH)$_2$ and Pt/Cd$_{1-x}$Zn$_x$S/Zn(OH)$_2$ were chosen based on our previous investigations due to their high photocatalytic activities [22,27]. The tendency toward increased photocatalytic activity with increasing ϵ-Zn(OH)$_2$ phase content in the composite photocatalysts was shown previously. In contrast, the presence of layered 2D β-Zn(OH)$_2$ was shown to decrease the photocatalytic activity of the composite Pt/Cd$_{1-x}$Zn$_x$S/ZnO/Zn(OH)$_2$ photocatalysts [22]. Unfortunately, the selected synthesis technique with low drying temperature ca. 70–80 °C does not allow the exclusion of 2D β-Zn(OH)$_2$ impurities, while increasing the temperature during synthesis reduces the photocatalytic activity of the samples due to the loss in the surface area. Thus, for these investigations, we chose four composite platinized samples: Cd$_{0.65}$Zn$_{0.35}$S/ϵ-Zn(OH)$_2$/2D β-Zn(OH)$_2$ (A), Cd$_{0.65}$Zn$_{0.35}$S/2D β-Zn(OH)$_2$ (B), Cd$_{0.4}$Zn$_{0.6}$S/ZnO/2D β-Zn(OH)$_2$ (C), and Cd$_{0.75}$Zn$_{0.25}$S/ZnO/2D β-Zn(OH)$_2$ (D) (Table 1). Additionally, single-phase Cd$_{0.6}$Zn$_{0.4}$S and 1%Pt Cd$_{0.6}$Zn$_{0.4}$S were used for experiments with the hydrogen evolution. Photocatalytic runs for the composite photocatalysts lasted 1.5 h and continued until the
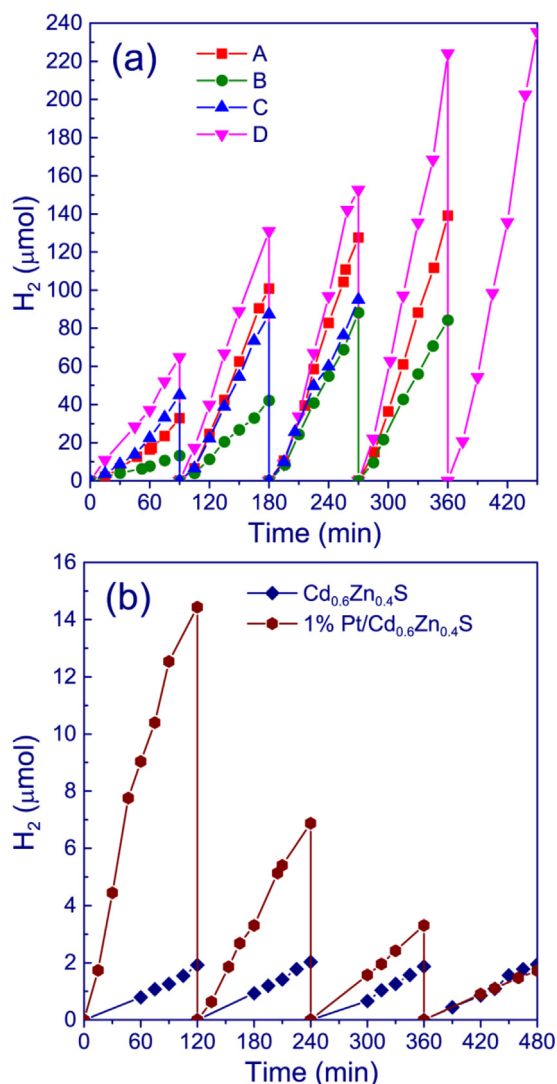

Fig. 1. Kinetics of hydrogen evolution for photocatalysts A–D (a), Cd$_{0.6}$Zn$_{0.4}$S and 1%Pt Cd$_{0.6}$Zn$_{0.4}$S (b). Conditions: C(C$_2$H$_5$OH) = 10 vol%, C(NaOH) = 0.1 M, C(cat) = 0.5 g/L, V = 100 mL, T = 20 °C, light source—450-nm LED.

rate changed within 5% (Fig. 1). For single-phase Cd$_{0.6}$Zn$_{0.4}$S and 1%Pt Cd$_{0.6}$Zn$_{0.4}$S, four 2-hour runs were performed.

Fig. 1a shows four consecutive hydrogen evolution runs for the four photocatalysts A–D. The activities of photocatalysts A–D as well as the activities of Cd$_{0.6}$Zn$_{0.4}$S and 1%Pt Cd$_{0.6}$Zn$_{0.4}$S are given in Table A.1 of Supplementary data. It should be noted that the kinetic curves of all platinized photocatalysts have an apparent induction period in the first run.

For single-phase Cd$_{0.6}$Zn$_{0.4}$S, no change in the hydrogen evolution rate is observed, whereas the 1%Pt/Cd$_{0.6}$Zn$_{0.4}$S photocatalyst undergoes a very strong deactivation, where the hydrogen evolution rate is decreased by a factor of 10 in 8 h. XPS investigations of fresh and deactivated samples of 1%Pt/Cd$_{0.6}$Zn$_{0.4}$S show the leaching of zinc on the surface of the photocatalyst (Table 2). A slight shift of peaks to lower angles in the XRD pattern of deactivated 1%Pt/Cd$_{0.6}$Zn$_{0.4}$S (Fig. A.3 of Supplementary data) also confirms a decrease in the zinc content. It was shown previously that the decrease in the x parameter in Cd$_{1-x}$Zn$_x$S when $x < 0.5$ leads to a reduced hydrogen evolution rate [22,28]. Additionally, cadmium and zinc mixed carbonate (Cd$_{0.92}$Zn$_{0.08}$CO$_3$) with a crystalline size approximately of 50 nm is formed, which can lead to a strong deactivation of the photocatalyst.

Table 2

Surface composition of photocatalyst 1 wt% Pt/Cd$_{0.6}$Zn$_{0.4}$S during photocatalytic hydrogen evolution, estimated by the XPS technique, mol%.

Sample	[Zn]/[Cd]	[Pt]/[Cd]	[S]/[Cd]	[Cd]/[Cd + Zn]	[Zn]/[Cd + Zn]	[S]/[Cd + Zn]	[Pt]/[Zn + Cd]
1%Pt/Cd$_{0.6}$Zn$_{0.4}$S	0.68	0.045	0.68	0.60	0.40	0.41	0.027
1%Pt/Cd$_{0.6}$Zn$_{0.4}$S[a]	0.25	0.034	0.68	0.80	0.20	0.54	0.027

[a] After photocatalytic hydrogen production (8 h).

One can see that the rate of H$_2$ evolution grows with the run number for all composite photocatalysts. The highest initial rate of hydrogen evolution is exhibited by photocatalyst D, which consists of Cd$_{0.75}$Zn$_{0.25}$S, ZnO, and 2D β-Zn(OH)$_2$. The high rate of hydrogen evolution can be attributed to good light adsorption and the formation of efficient heterojunctions between sulfide and zinc oxide nanoparticles at the molar fractions of the components in photocatalyst D. The position of the conduction band (CB) of ZnO is −0.1 V vs. NHE (normal hydrogen electrode) [29], whereas the position of Cd$_{0.75}$Zn$_{0.25}$S CB is ca. −0.42 V vs. NHE [30]; thus, under visible light irradiation, photogenerated electrons from the CB of Cd$_{0.75}$Zn$_{0.25}$S can transfer to the CB of zinc oxide, and holes can transfer from the VB of ZnO to the VB of the solid solution of zinc and cadmium sulfides. It is well known that efficient charge separation at heterojunctions decreases electron-hole recombination and enhances photocatalytic activity [27,31]. The rate of hydrogen evolution on single-phase platinized 1%Pt/Cd$_{0.6}$Zn$_{0.4}$S in the first run is lower than on photocatalysts A, C, and D but higher that on photocatalyst B. The activity of photocatalyst B (Pt/Cd$_{0.65}$Zn$_{0.35}$S/2D β-Zn(OH)$_2$) is quite low due to the high 2D β-Zn(OH)$_2$ content, which is not effective for heterojunction formation [22], and the absence of ZnO and ε-Zn(OH)$_2$.

Fig. 1a shows that for the multi-phase photocatalysts, a strong activation is observed. The activation time varies from 3 to 6 h for different photocatalysts. XRD patterns of the samples before and after hydrogen production were obtained to explain the activation of the photocatalysts. Fig. 2a–b shows the transformation of the XRD patterns of photocatalysts during hydrogen evolution. According to the XRD data, the two main Zn-containing phases in the samples are ε-Zn(OH)$_2$ and ZnO (wurtzite-like structure). Broad peaks located at 25–30 are attributed to Cd$_{1−x}$Zn$_x$S with disordered structure; the broad peak at 2θ = 33° has been previously attributed to layered 2D β-Zn(OH)$_2$ [22].

For all samples, the ε-Zn(OH)$_2$ content grows, whereas 2D β-Zn(OH)$_2$ disappears. Additionally, for samples B and D, the zinc oxide content grows slightly. The positions of the broad peaks of Cd$_{1−x}$Zn$_x$S do not change; thus, the Zn and Cd contents in sulfide solid solution remain unchanged during photocatalytic hydrogen evolution. The UV–vis spectra of photocatalysts B and C before and after photocatalytic runs were obtained (Fig A.4 of Supplementary data). Fig A.4 of Supplementary data shows that the adsorption edge shifts to longer wavelengths by approximately 10 nm for both photocatalysts. This red-shift may be caused by the disappearance of layered 2D β-Zn(OH)$_2$ from the surface of the photocatalyst, as the presence of layered zinc hydroxide increases the band gap energy [32]. According to well-known mechanism of Ostwald ripening [33], small crystals or sol particles dissolve, and redeposit onto larger crystals or sol particles. Thus, relatively small nanoparticles of 2D β-Zn(OH)$_2$ can dissolve in an alkaline medium and then deposit on the surface of ε-Zn(OH)$_2$ because the solubility of layered 2D β-Zn(OH)$_2$ is higher as compared to solubility of ε-Zn(OH)$_2$ due to the difference in the particle size. As was described before [32], β-Zn(OH)$_2$ is a metastable modification, therefore ε-Zn(OH)$_2$ can be formed after the recrystallization.

Earlier it was shown that the formation of heterojunctions is possible between Cd$_{0.6}$Zn$_{0.4}$S and ε-Zn(OH)$_2$ [22]. Thus, the presence of ε−Zn(OH)$_2$ can improve the activity of the composite photocatalyst. In contrast, 2D β-Zn(OH)$_2$ phase is not beneficial for

the photocatalytic activity. The presence of layered β-Zn(OH)$_2$ on the surface of ZnO quantum dots drastically increases the photoluminescence intensity in the range 500–550 nm [32]. Thus, if the surface of the composite photocatalyst is covered by 2D β-Zn(OH)$_2$ the electron-hole pair recombination is quite high and the quantum activity is low.

The highest (5-fold) increase in activity is achieved in the case of photocatalyst B, which transforms from Pt/Cd$_{0.65}$Zn$_{0.35}$S/2D β-Zn(OH)$_2$ to Pt/Cd$_{0.65}$Zn$_{0.35}$S/ε-Zn(OH)$_2$/ZnO. For samples A and D, the activity increased by a factor of 3.1–3.4, and for sample C the increase was ca. 42%. The increase in the photocatalytic activity of sample C is not significant, because the initial 2D β-Zn(OH)$_2$ content, which can transform to ZnO and ε-Zn(OH)$_2$, is low. Moreover, unidentified impurities with interplanar spacings of 3.33 and 1.67 Å (Fig 2b) may negatively affect the photocatalytic activity. The highest rate of hydrogen evolution, 2.86 μmol/min, is achieved by photocatalyst D, consisting of Cd$_{0.75}$Zn$_{0.25}$S (∼20 wt%), ZnO (∼60 wt%), and ε-Zn(OH)$_2$ (∼20 wt%) at the end of the 5th photocatalytic run. Triple heterojunctions [22] are likely formed in this composite photocatalyst, leading to the high rate of hydrogen evolution.

The experiments performed confirm the assumption that ε-Zn(OH)$_2$ and ZnO phases with good crystallinity are required for efficient hydrogen evolution. It is worth noting that the activity of sample D in the 3rd and 4th photocatalytic runs is equal to 3400 μmol g^{-1} h^{-1} and AQE is equal to 12.4%, which exceeds (Table A.2 of Supplementary data) the activities reported for hydrogen evolution from aqueous solutions of alcohols under visible light in previous papers [22,27,34–37]. However, it should be noted that LED is used as a light source in present work that also can enhance the rate of the hydrogen evolution.

3.2. Detailed investigations of photocatalyst A

Detailed experiments on the activation and deactivation of photocatalyst A were conducted, including long-term 60-hour experiments. Photocatalyst A was chosen because at the beginning of the reaction, it consists of two crystalline phases, Cd$_{0.65}$Zn$_{0.35}$S as well as ε-Zn(OH)$_2$ and layered 2D β-Zn(OH)$_2$, while after activation, it consists of Cd$_{0.65}$Zn$_{0.35}$S and ε-Zn(OH)$_2$. Only traces of ZnO (ca. 3%) are identified in this sample before and after hydrogen evolution. Thus, the transformation of photocatalyst A is more easily described in comparison to photocatalysts C and D. At the same time, photocatalyst A is more active than photocatalyst B.

Fig. 3 shows the rates of hydrogen evolution on photocatalyst A during twelve 5-hour runs. The rate achieves the maximum in the third run and then falls very slowly (ca. 15% after 40 h) until the 10th run. Deactivation occurs in the 10th run, after 60 h of hydrogen production. To explain the activation and deactivation processes, the XRD patterns of photocatalyst A after each 1.5-hour run (Fig. 1) and after twelve 5-hour runs of hydrogen production (Fig. 3) were obtained and compared with the XRD pattern of the fresh photocatalyst (Fig. 2a). The ε-Zn(OH)$_2$ content increases with reaction time until 6 h and then remains almost unchanged. Additionally, the CdCO$_3$ peaks appear in the XRD pattern after 60 h of the reaction. Table 3 and Fig. 4 show the bulk and surface composition of photocatalyst A during photocatalytic hydrogen evolution, as estimated by XRD and XPS techniques. In addition to the increasing
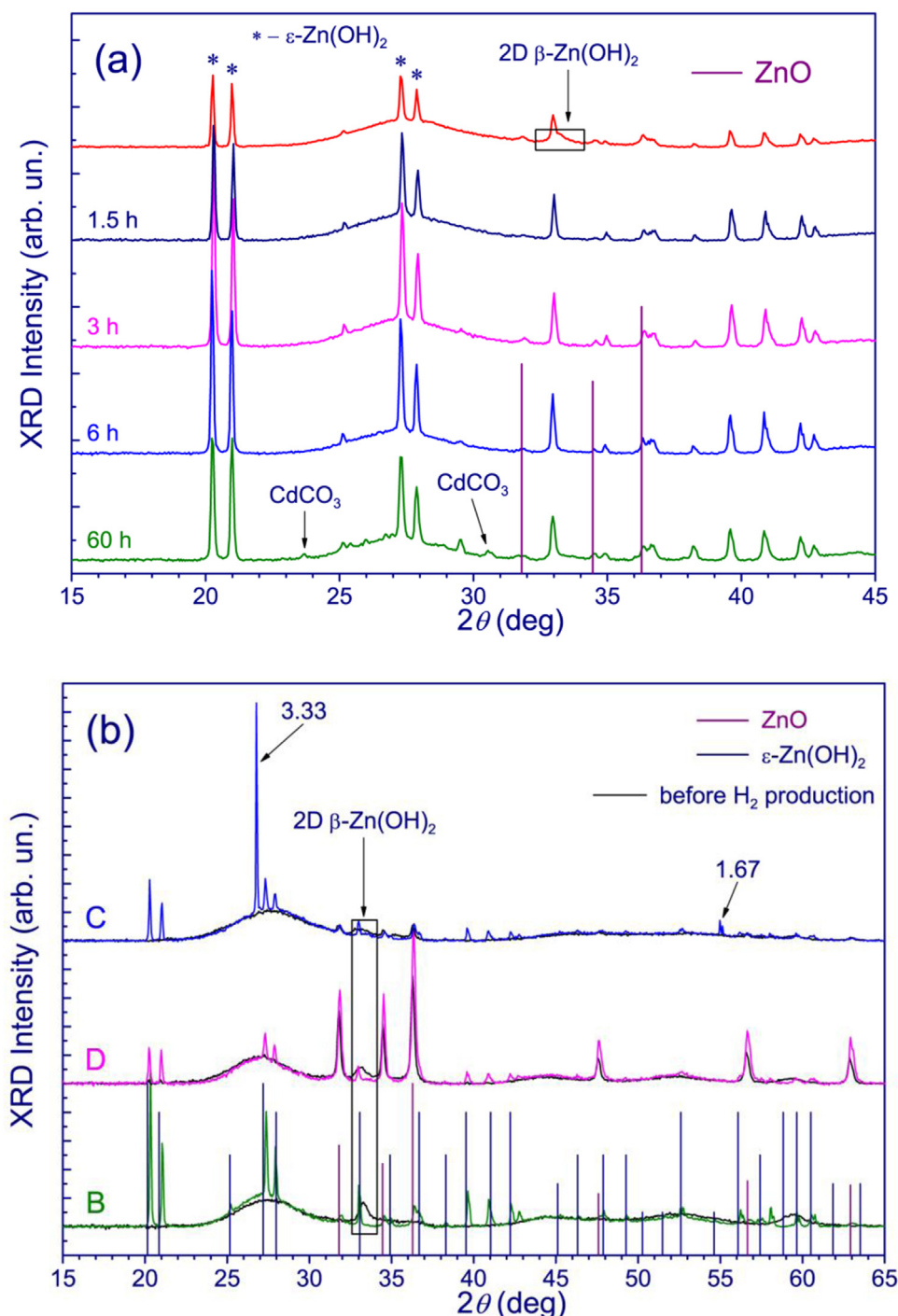
Fig. 2. The transformation of XRD patterns of photocatalysts A (a, red line—fresh photocatalyst), B, C, and D (b, black line— fresh photocatalyst) during hydrogen production. (For interpretation of the references to colour in this figure legend, the reader is referred to the web version of this article.)

ϵ-Zn(OH)$_2$ content and the disappearance of 2D β-Zn(OH)$_2$, the Cd$_{0.65}$Zn$_{0.35}$S content decreases. XPS investigations of photocatalyst A show that the surface sulfide content grows in the first 1.5 h of the reaction and then begins to fall, whereas XRD analysis reveals that the bulk sulfide content decreases monotonically during the reaction. Thus, a partial dissolution of Cd$_{0.65}$Zn$_{0.35}$S with the further formation of zinc hydroxide and cadmium carbonate occurs.

In addition to the phase composition, the state of platinum can affect the photocatalytic activity [38]. Fig. 5 shows the dependences of the surface [Pt]/[Cd + Zn] molar ratio and the value of the Pt4$f_{7/2}$ binding energy calculated by XPS technique on the reaction time. These curves are almost identical; thus, the surface platinum content varies simultaneously with the Pt4$f_{7/2}$ binding energy. According to the literature, the Pt4$f_{7/2}$ binding energy of bulk metallic platinum is 71.1–71.2 eV [39], whereas the Pt4$f_{7/2}$ binding energies of PtO, PtO$_2$, and Pt(OH)$_4$ are in the ranges of 72.25–72.4 eV [40], 74.0–74.1 eV [41], and 74.2–74.4 eV [41], respectively. Consequently, the platinum on the surface of both fresh and deactivated photocatalysts can be assumed to exist in a metallic state, Pt^0. One may observe an increase in the Pt4$f_{7/2}$ binding energy at the beginning of the reaction from 71.2 to 71.5 eV, likely because of an increase in nanoparticle dispersity. It was previously shown that
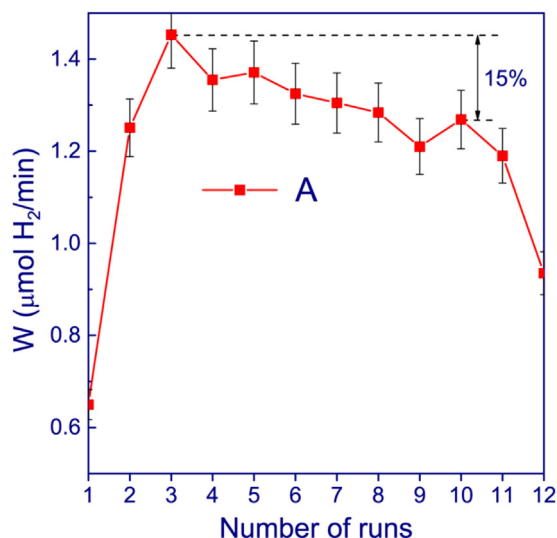
Fig. 3. Rates of hydrogen evolution on photocatalyst A during 12 5-hour runs. Conditions: $C(C_2H_5OH) = 10$ vol%, $C(NaOH) = 0.1$ M, $C(cat) = 0.5$ g/L, $V = 100$ mL, $T = 20\,°C$, light source—450-nm LED.

Fig. 4. Bulk and surface sulfide content during photocatalytic hydrogen evolution (mol%) calculated by XRD and XPS techniques (left Y axis) and the hydrogen evolution rate (dotted line, right Y axis).

the Pt$4f_{7/2}$ binding energy grows with decreasing metal nanoparticle size [42]. At the end of the reaction, the Pt$4f_{7/2}$ binding energy falls to 71.0 eV, indicating an aggregation of the platinum nanoparticles. The surface Pt content is intrinsically linked to its dispersion, as confirmed by the dependence of the [Pt]/[Cd + Zn] molar ratio on the reaction time. HRTEM images of fresh and deactivated photocatalyst A were obtained and Pt particle size distributions were calculated to confirm the aggregation of platinum nanoparticles (Fig. 6). Fresh photocatalyst has narrow Pt particle size distribution on with a maximum at 1.3 nm. After 60 h of the hydrogen evolution
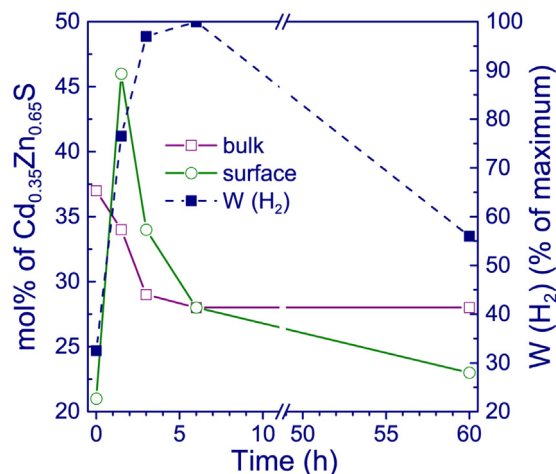
the particle size distribution becomes broader, the maximum shifts to 1.7 nm. The deactivation of a photocatalyst due to the aggregation of platinum nanoparticles was previously shown for Pt/TiO$_2$ [38], and thus, in the case of photocatalyst A, the aggregation of platinum may also contribute to the deactivation.

It should be noted that the rate of hydrogen evolution achieves its maximum at 4.5–6 h of the reaction, whereas the maximum Cd$_{0.65}$Zn$_{0.35}$S and Pt surface content occurs at 1.5–3 h of the reaction. Fig. 4 shows that the curve of the hydrogen evolution rate proceeds generally later than the curve of Cd$_{0.65}$Zn$_{0.35}$S surface content. Therefore, there is no direct connection between the surface sulfide or platinum content and the rate of hydrogen evolution.

Table 3
Bulk and surface composition of photocatalyst A during photocatalytic hydrogen evolution, estimated by the XRD and XPS techniques.

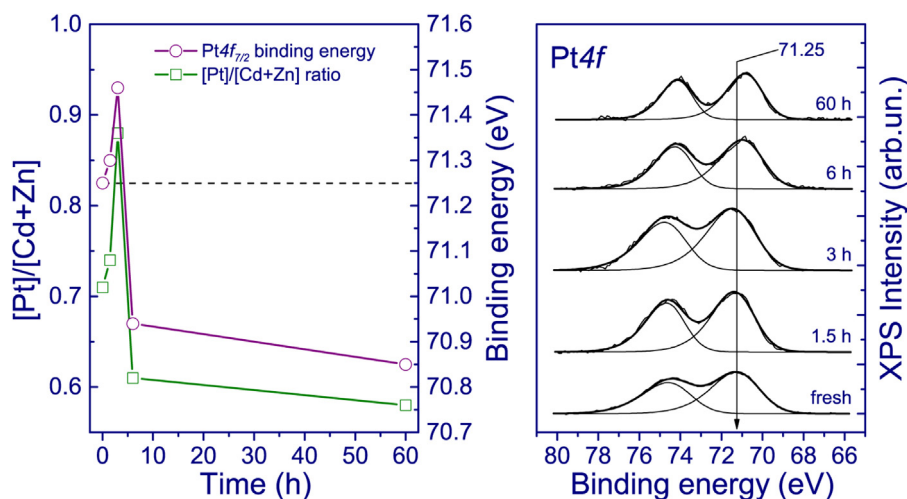| Time, h	Bulk						Surface		
	Cd$_{1-x}$Zn$_x$S	x	ZnO	ϵ-Zn(OH)$_2$	β-Zn(OH)$_2$	CdCO$_3$	[Cd]/[Cd + Zn],%	[S]/[Cd + Zn], %	[Pt]/[Cd + Zn], %
0	37	0.35	3	45	15	–	18	21	0.71
1.5	34	0.35	3	63	0	–	47	46	0.74
3	29	0.35	3	68	0	–	37	34	0.88
6	28	0.35	3	69	0	–	25	28	0.61
60	28	0.35	3	66	0	3	21	23	0.58

Fig. 5. Dependences of surface platinum to cadmium and zinc molar ratio and Pt$4f_{7/2}$ binding energy on reaction time, calculated by the XPS technique (left), and the Pt$4f_{7/2}$ spectra (right).
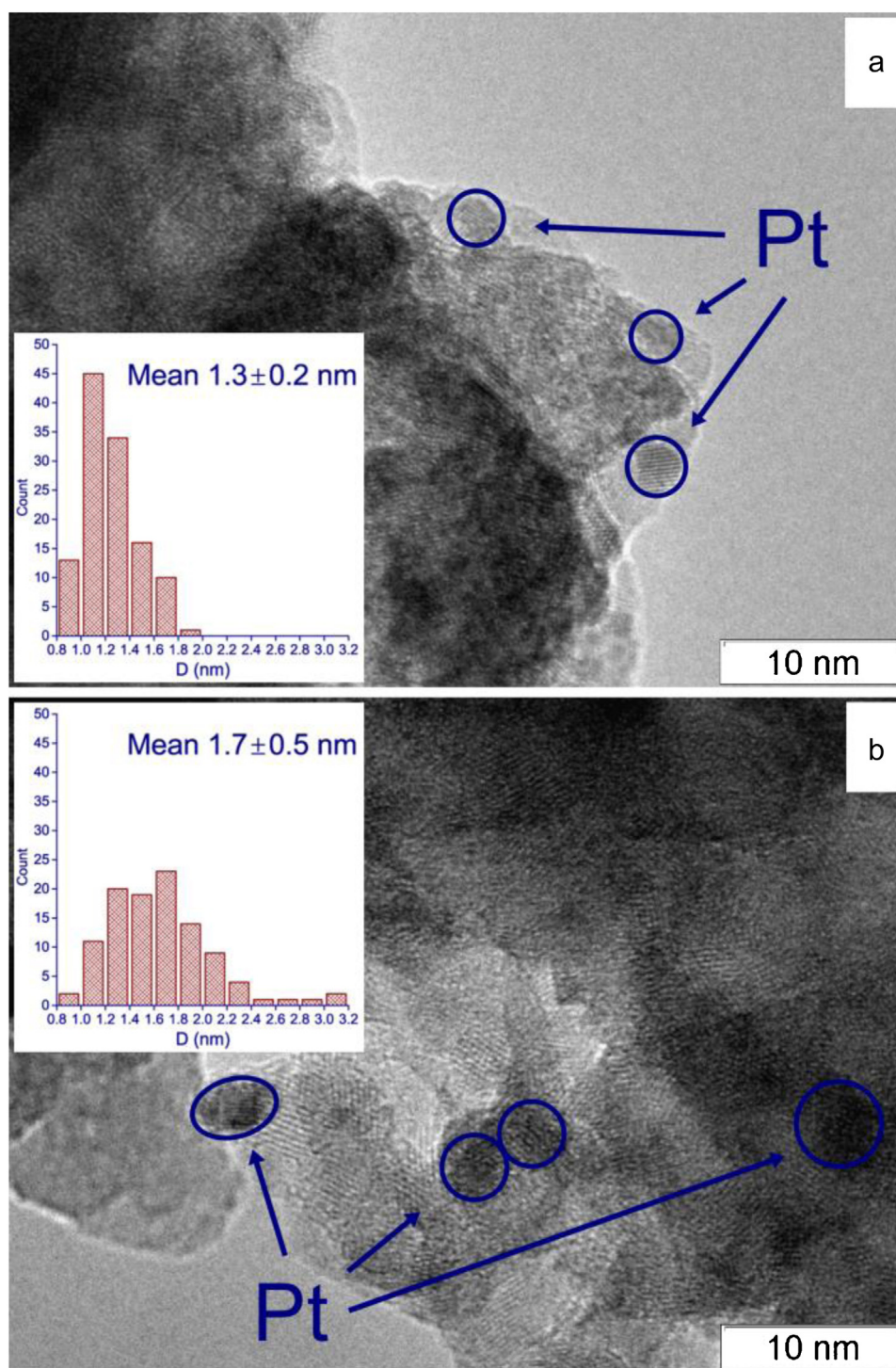
Fig. 6. HTREM images of fresh (a) and deactivated (b) photocatalysts A with Pt particle size distribution.

The dependence of the hydrogen evolution rate on the ϵ-Zn(OH)$_2$ content was obtained (Fig. 7) for fresh and activated/deactivated photocatalysts A and activated photocatalyst B. Photocatalysts A and B were selected for comparison because they have similar values of $x = 0.35$ in Cd$_{1-x}$Zn$_x$S and likely similar molar Cd$_{0.65}$Zn$_{0.35}$S content. Fig. 7 shows that the rate of the hydrogen evolution grows linearly with the ϵ-Zn(OH)$_2$ content. Only one point—photocatalyst A after 60 h—falls outside the general dependence. This low rate may be caused by the presence of CdCO$_3$ and dissolution of Cd$_{0.65}$Zn$_{0.35}$S in the photocatalyst after 60 h of the reaction. Thus, for photocatalysts Cd$_{0.65}$Zn$_{0.35}$S/ϵ-Zn(OH)$_2$, the rate of hydrogen evolution grows with the ϵ-Zn(OH)$_2$ content. For photocatalysts C and D, their activity also grows with the ϵ-Zn(OH)$_2$ content. However, for these photocatalysts, it is not possible to find the direct dependence of the rate on the ϵ-Zn(OH)$_2$ content. At the beginning of the illumination, photocatalysts C and D consist of two crystalline phases, Cd$_{1-x}$Zn$_x$S and ZnO, whereas after the activation, these catalysts contain three crystalline phases: Cd$_{1-x}$Zn$_x$S, ZnO, and ϵ-Zn(OH)$_2$. Thus, at the end of the reaction, the triple heterojunctions described earlier [22] can exist.
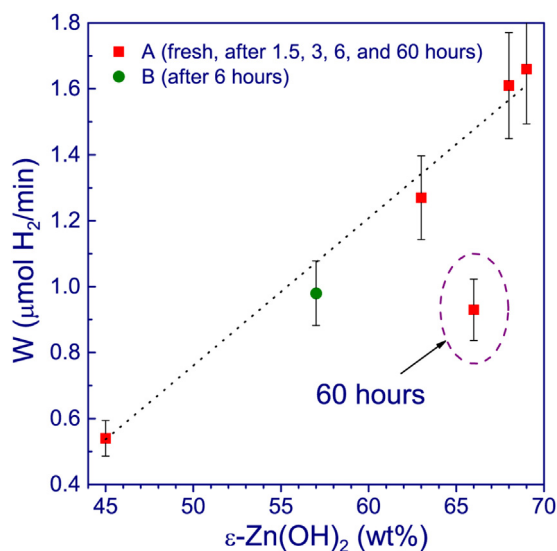
Fig. 7. Dependence of hydrogen evolution rate on molar ϵ-Zn(OH)$_2$ content in 0.44%Pt/Cd$_{0.65}$Zn$_{0.35}$S/ZnO/ϵ-Zn(OH)$_2$. Conditions: C(C$_2$H$_5$OH) = 10 vol%, C(NaOH) = 0.1 M, C(cat) = 0.5 g/L, V = 100 mL, T = 20 °C, light source —450-nm LED.
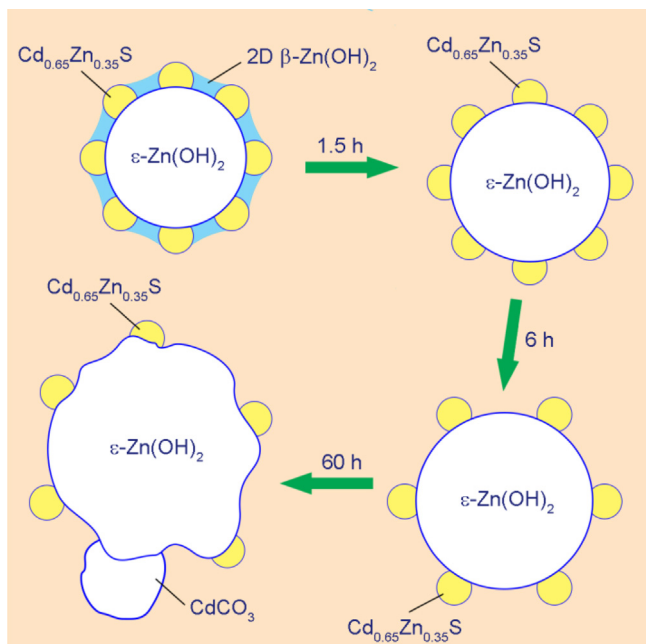

Fig. 8. Schematic mechanism of the transformation of photocatalyst A.

XRD and XPS data analysis suggests the following schematic mechanism of the transformation of photocatalyst A (Fig. 8). At the beginning, layered β-Zn(OH)$_2$, which likely covers the surface of Cd$_{0.65}$Zn$_{0.35}$S, transforms to ϵ-Zn(OH)$_2$ with a high crystalline size, releasing the surface of the sulfide. Simultaneously, the dispersion of platinum nanoparticles grows at the beginning of the hydrogen evolution and then begins to fall after 3 h of the reaction. These processes initially increase the rate of hydrogen production. Then, the dissolution of Cd$_{0.65}$Zn$_{0.35}$S occurs on the surface of the photocatalyst, leading to a slight loss of photocatalytic activity. At the end of our experiments, CdCO$_3$ forms on the surface of the photocatalysts, whereas ϵ-Zn(OH)$_2$ content begins to fall, and deactivation occurs.

According to the proposed transformation mechanism (Fig. 8) the surface of ϵ-Zn(OH)$_2$ is completely covered by 2D β-Zn(OH)$_2$ whereas the surface of Cd$_{0.6}$Zn$_{0.4}$S is partially covered by 2D β-Zn(OH)$_2$ in fresh photocatalyst A. HRTEM image of fresh pho-

tocatalysts A with EDX spectrum from the site without Cd$_{0.6}$Zn$_{0.4}$S is shown in Fig. 5A of Supplementary data (top). Under conditions of the TEM experiments both β-Zn(OH)$_2$ and ϵ-Zn(OH)$_2$ transform into zinc oxide. EDX spectrum confirms that at this site there is no cadmium sulfide. Therefore, TEM image represents ZnO nanoparticles only. However, one can see two types of particles: a large one with the crystallite size more than 50 nm and laminated particles with the crystallite size ~10 nm. It can confirm the assumption that before the experiment the surface of ϵ-Zn(OH)$_2$ is covered by 2D β-Zn(OH)$_2$. Fig. 5A of Supplementary data (bottom) shows HRTEM image of fresh photocatalysts A with EDX spectrum from the site with both Cd$_{0.65}$Zn$_{0.35}$S and ZnO. It is quite difficult to distinguish zinc oxide nanoparticles on the surface of Cd$_{0.65}$Zn$_{0.35}$S due to the higher molar mass of sulfide. However, one can see small particles of zinc oxide on the surface of the photocatalyst. These nanoparticles are likely formed from 2D β-Zn(OH)$_2$ under conditions of the TEM experiments. Previously published results show that after several minutes of calcination at 300 °C large and small particles of ZnO are formed from ϵ-Zn(OH)$_2$ and 2D β-Zn(OH)$_2$ respectively [22]. The XPS investigations (Table 3) show that the surface concentration both of sulfur and cadmium is increased by a factor of 2 after first run whereas XRD patterns represent that the bulk content of Cd$_{0.6}$Zn$_{0.4}$S slightly falls, simultaneously all 2D β-Zn(OH)$_2$ transforms to ϵ-Zn(OH)$_2$. Thus, one can assume that in the fresh photocatalyst the surface of Cd$_{0.6}$Zn$_{0.4}$S is partially covered by 2D β-Zn(OH)$_2$.

The mechanism of Pt/Cd$_{0.6}$Zn$_{0.4}$S activation/deactivation is likely the same: the activation at the beginning (15 min) of the first run is caused by the increased dispersion of platinum nanoparticles, and later deactivation is associated the formation of Cd$_{0.92}$Zn$_{0.8}$CO$_3$. According to the mechanism proposed by de Oliveira Melo et al. for the hydrogen evolution from aqueous solutions of glycerol over Pt/CdS and Pt/CdS/TiO$_2$, on the first stage of the reaction, CO evolves from C$_3$H$_8$O$_3$ and poisons the surface of the photocatalyst [26]. Further, active oxygen species are formed after the reaction of water with photogenerated holes and oxidize CO to CO$_2$. The removal of carbon monoxide from the surface leads to an increase in the hydrogen evolution rate [26]. The formation and further oxidation of carbon monoxide on the surface of the photocatalyst can affect the dispersion of platinum nanoparticles. We analyzed the gas phase after the first run of the hydrogen evolution over Pt/Cd$_{0.6}$Zn$_{0.4}$S and carbon monoxide was detected. The molar ratio of H$_2$ to CO was 0.18, thus, the amount of carbon oxide is quite high. Carbon dioxide is not identified in the gas phase because it reacts with NaOH in the suspension.

The likely mechanism of cadmium carbonate formation is as follows. Oxidation of CdS by photogenerated holes can lead to the release of Cd^{2+} and SO$_4$$^{2-}$ ions to the aqueous solution [43]. Simultaneously, in an alkaline medium (pH 13), carbonate ions can be formed from carbon dioxide, which exists in air or is formed in hydrogen evolution from aqueous solutions of ethanol according to the following equation:

$$C_2H_5OH + 3H_2O \rightarrow 6H_2 + 2CO_2.$$
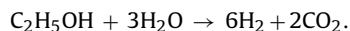
Cadmium carbonate has a very low solubility constant (5.2×10^{-12} M^{-1} at 25 °C), which facilitates its formation in the reaction solution.

It worth noting that the cadmium carbonate content in deactivated photocatalyst A after 60 h of hydrogen evolution is lower than in deactivated Pt/Cd$_{0.6}$Zn$_{0.4}$S after 8 h of hydrogen evolution. Thus, the composite photocatalysts Pt/Cd$_{1-x}$Zn$_x$S/ZnO/Zn(OH)$_2$ have improved both photocatalytic activity and stability. The amount of hydrogen evolved on 50 mg of photocatalyst A in 12 runs was equal to 4.4 mmol or 107 mL of H$_2$.

4. Conclusions

The novel composite photocatalysts Pt/Cd$_{1-x}$Zn$_x$S/ZnO/Zn(OH)$_2$ and Pt/Cd$_{1-x}$Zn$_x$S/ZnO, with high activity under visible light, were studied in cyclic experiments on photocatalytic hydrogen production under visible light. The activation of the composite photocatalysts during photocatalytic hydrogen evolution from alkaline aqueous solutions of ethanol was observed. The rate increase for the platinized multiphase photocatalysts varies from 40 to 500%, whereas the activity of single phase Pt/Cd$_{1-x}$Zn$_x$S decreases drastically after 8 h of hydrogen evolution. The activation is likely caused by the in situ formation of ϵ-Zn(OH)$_2$ and the disappearance of layered 2D β-Zn(OH)$_2$ in a basic medium. Additionally, an increase in platinum dispersity is observed during the reaction. Photocatalysts 0.44%Pt/Cd$_{0.65}$Zn$_{0.35}$S/ZnO/ϵ-Zn(OH)$_2$ possess a high stability during 50 h of the photocatalytic reaction. The deactivation of Pt/Cd$_{0.65}$Zn$_{0.35}$S/ZnO/Zn(OH)$_2$ after 60 h of the hydrogen evolution, like the deactivation of single-phase 1%Pt/Cd$_{0.6}$Zn$_{0.4}$S, is caused by CdCO$_3$ formation and the partial dissolution of Cd$_{1-x}$Zn$_x$S. The composite photocatalysts are shown to be much more stable than platinized single-phase cadmium and zinc sulfide solid solution.

Acknowledgment

Appendix A. Supplementary data

Supplementary data associated with this article can be found, in the online version, at http://dx.doi.org/10.1016/j.apcatb.2015.10.042.

References

[1] K.I. Zamaraev, V.N. Parmon, Catal. Rev. Sci. Eng. 22 (1980) 261–324.
[2] J.A. Turner, Science 305 (2004) 972–974.
[3] M. Cargnello, A. Gasparotto, V. Gombac, T. Montini, D. Barreca, P. Fornasiero, Eur. J. Inorg. Chem. (2011) 4309–4323.
[4] S. Zinoviev, F. Mueller-Langer, P. Das, N. Bertero, P. Fornasiero, M. Kaltschmitt, G. Centi, S. Miertus, ChemSusChem 3 (2010) 1106–1133.
[5] A. Fujishima, K. Honda, Nature 238 (1972) 37–38.
[6] X. Li, J. Yu, J. Low, Y. Fang, J. Xiao, X. Chen, J. Mater. Chem. A 3 (2015) 2485–2534.
[7] E.A. Kozlova, A.V. Vorontsov, Int. J. Hydrogen Energy 35 (2010) 7337–7343.
[8] Y.X. Li, G.X. Lu, S.B. Li, Appl. Catal. A 214 (2001) 179–185.
[9] Y.X. Li, Y.Z. Me, S.Q. Peng, G.X. Lu, S.B. Li, Chemosphere 63 (2006) 1312–1318.
[10] Y.X. Li, G.X. Lu, S.B. Li, Chemosphere 52 (2003) 843–850.
[11] A. Patsoura, D.I. Kondarides, X.E. Verykios, Appl. Catal. B 64 (2006) 171–179.
[12] M. Stylidi, D.I. Kondarides, X.E. Verykios, Appl. Catal. B 47 (2004) 189–201.
[13] D.I. Kondarides, V.M. Daskalaki, A. Patsoura, X.E. Verykios, Catal. Lett. 122 (2008) 26–32.
[14] G.N. Nomikos, P. Panagiotopoulou, D.I. Kondarides, X.E. Verykios, Appl. Catal. B 146 (2014) 249–257.
[15] A. Petala, E. Ioannidou, A. Georgaka, K. Bourikas, D.I. Kondarides, Appl. Catal. B 178 (2015) 201–209.
[16] Q. Gu, X. Fu, X. Wang, Sh. Chen, D.Y.C. Leung, X. Xie, Appl. Catal. B 106 (2011) 689–696.
[17] J. Ran, J. Zhang, J. Yu, S.Zh. Qiao, ChemSusChem 7 (2015) 3426–3434.
[18] X. Zong, H.J. Yan, G.P. Wu, G.J. Ma, F.Y. Wen, L. Wang, C. Li, J. Am. Chem. Soc. 130 (2008) 7176–7177.
[19] Q. Li, H. Meng, P. Zhou, Y. Zheng, J. Wang, J. Yu, J.R. Gong, ACS Catal. 3 (2013) 882–889.
[20] C. Dinh, M. Pham, Y. Seo, F. Kleitz, T. Do, Nanoscale 6 (2014) 4819–4829.
[21] Y.A. Gruzdkov, E.N. Savinov, V.V. Korolkov, V.N. Parmon, React. Kinet. Catal. Lett. 36 (1988) 395–400.
[22] E.A. Kozlova, D.V. Markovskaya, S.V. Cherepanova, A.A. Saraev, E. Yu Gerasimov, T.V. Perevalov, V.V. Kaichev, V.N. Parmon, Int. J. Hydrogen Energy 39 (2014) 18758–18769.
[23] Y. Li, D. Gao, Sh. Peng, G. Lu, Sh. Li, Int. J. Hydrogen Energy 36 (2011) 4291–4297.
[24] V. Gombac, L. Sordelli, T. Montini, J.J. Delgado, A. Adamski, G. Adami, M. Cargnello, S. Bernal, P. Fornasiero, J. Phys. Chem. A 114 (2010) 3916–3925.
[25] V.M. Daskalaki, D.I. Kondarides, Catal. Today 144 (2009) 75–80.
[26] M. de Oliveira Melo, L. Almeida Silva, J. Photochem. Photobiol. A 226 (2011) 36–41.
[27] T.P. Lyubina, D.V. Markovskaya, E.A. Kozlova, E.A.V.N. Parmon, Int. J. Hydrogen Energy 38 (2013) 14172–14179.
[28] T.P. Lyubina, E.A. Kozlova, Kinet. Catal. 53 (2012) 188–196.
[29] D. Jing, L. Guo, L. Zhao, X. Zhang, H. Liu, M. Li, Sh. Shen, G. Liu, X. Hu, X. Zhang, K. Zhang, L. Ma, P. Guo, Int. J. Hydrogen Energy 35 (2010) 7087–7097.
[30] C. Xing, Y. Zhang, W. Yan, L. Guo, Int. J. Hydrogen Energy 31 (2006) 2018–2024.
[31] H.X. Sang, X.T. Wang, C.C. Fan, Int. J. Hydrogen Energy 37 (2012) 1348–1355.
[32] H. Zhou, H. Alves, D.M. Hoffman, W. Kriegseis, B.K. Meyer, G. Kaczmarczyk, A. Hoffman, Appl. Phys. Lett. 80 (2002) 210–212.
[33] W. Ostwald, Z. Phys. Chem. 22 (1897) 289–330.
[34] X. Zhou, Z. Luo, P. Tao, B. Jin, Z. Wu, Y. Huang, Mater. Chem. Phys. 143 (2014) 1462–1468.
[35] N. Strataki, M. Antoniadou, V. Dracopoulos, P. Kianos, Catal. Today 151 (2010) 53–57.
[36] Y. Yang, E. Liu, H. Dai, L. Kang, H. Wu, J. Fan, X. Hu, H. Liu, Int. J. Hydrogen Energy 39 (2014) 7664–7671.
[37] W. Zhao, Z. Ai, X. Zhu, M. Zhang, Q. Shi, J. Dai, Int. J. Hydrogen Energy 39 (2014) 7705–7712.
[38] E.A. Kozlova, T.P. Lyubina, M.A. Nasalevich, A.V. Vorontsov, A.V. Miller, V.V. Kaichev, V.N. Parmon, Catal. Commun. 12 (2011) 597–601.
[39] A.V. Miller, V.V. Kaichev, I.P. Prosvirin, V.I. Bukhtiyarov, J. Phys. Chem. C 117 (2013) 8189–8197.
[40] G.M. Bancroft, I. Adams, L.L. Coatsworth, C.D. Bennewitz, J.D. Brown, W.D. Westwood, Anal. Chem. 47 (1975) 586–588.
[41] M. Peuckert, H.P. Bonzel, Surf. Sci. 145 (1984) 239–259.
[42] M.G. Mason, Phys. Rev. B 27 (1983) 748–762.
[43] D. Meissner, R. Memming, L. Shuben, S. Yesodharan, M. Graetzel, Ber. Bunsenges. Phys. Chem. 89 (1985) 121–124.